

Neutron excitations in ^{119}Ba

K. K. Zheng,^{1,2} C. M. Petrache,¹ Z. H. Zhang,³ A. Astier,¹ B. F. Lv,^{1,*} P. T. Greenlees,⁴ T. Grahm,⁴ R. Julin,⁴ S. Juutinen,⁴ M. Luoma,⁴ J. Ojala,⁴ J. Pakarinen,⁴ J. Partanen,^{4,†} P. Rähkila,⁴ P. Ruotsalainen,⁴ M. Sandzelius,⁴ J. Sarén,⁴ H. Tann,^{4,5} J. Uusitalo,⁴ G. Zimba,⁴ B. Cederwall,⁶ Ö. Aktas,⁶ A. Ertoprak,⁶ W. Zhang,⁶ S. Guo,^{2,7} M. L. Liu,^{2,7} X. H. Zhou,^{2,7} I. Kuti,⁸ B. M. Nyakó,⁸ D. Sohler,⁸ J. Timár,⁸ C. Andreoiu,⁹ M. Doncel,⁵ D. T. Joss,⁵ and R. D. Page⁵

¹*Université Paris-Saclay, CNRS/IN2P3, IJCLab, 91405 Orsay, France*

²*Key Laboratory of High Precision Nuclear Spectroscopy and Center for Nuclear Matter Science, Institute of Modern Physics, Chinese Academy of Sciences, Lanzhou 730000, People's Republic of China*

³*Mathematics and Physics Department, North China Electric Power University, Beijing 102206, China*

⁴*University of Jyväskylä, Department of Physics,*

P.O. Box 35, FI-40014, University of Jyväskylä, Finland

⁵*Oliver Lodge Laboratory, Department of Physics,*

University of Liverpool, Liverpool L69 7ZE, United Kingdom

⁶*KTH Department of Physics, S-10691 Stockholm, Sweden*

⁷*School of Nuclear Science and Technology, University of Chinese*

Academy of Science, Beijing 100049, People's Republic of China

⁸*Institute for Nuclear Research (Atomki-ELKH), 4001 Debrecen, Hungary*

⁹*Department of Chemistry, Simon Fraser University, Burnaby, BC V5A 1S6, Canada*

(Dated:)

The neutron-deficient ^{119}Ba nucleus has been studied using the $^{58}\text{Ni}(^{64}\text{Zn}, 2pn)$ reaction and the JUROGAM 3 gamma-ray detector array coupled to the MARA recoil-mass separator setup. One new rotational band and several low-lying states are newly identified. A half-life of $T_{1/2} = 0.36(2) \mu\text{s}$ has been measured for the $5/2^-$ band-head of the $\nu h_{11/2}$ band. The two previously known rotational bands are confirmed, excepting the higher part of the positive-signature partner of the positive-parity band. Configurations are assigned based on the analysis of the observed quasi-particle alignments whose nature is unveiled by the calculations using the particle number conserving cranked shell model.

PACS numbers: 21.10.Re, 21.60.Ev, 23.20.Lv, 27.60.+j

I. INTRODUCTION

The study of the lightest Ba nuclei is confronted with the increasing difficulty to populate high-spin states using fusion-evaporation reactions, due to the limited choice of projectile-target combinations and the small cross-sections for the evaporation of neutrons close to the proton drip-line. The existing experimental information on high-spin states in very proton-rich nuclei is therefore increasingly scarce towards the proton-drip line. The lightest odd-even $^{117,119}\text{Ba}$ nuclei with known rotational bands have been studied using the high-efficiency γ -detector array GAMMASPHERE [1] coupled with the recoil mass separator FMA [2] employing the fusion-evaporation the $^{64}\text{Zn}(^{58}\text{Ni}, 2pxn)$ reaction [3, 4], while ^{121}Ba has been studied using a complex setup consisting of the γ -detector array NORDBALL consisting of 15 Compton-suppressed Ge detectors and ancillary detectors for neutrons and protons employing

the $^{92}\text{Mo}(^{32}\text{S}, p2n)$ reaction [5]. Two or three rotational bands have been observed in these odd-even Ba nuclei, but not detailed spectroscopy of the low-lying states was performed until now.

The present work is devoted to the study of ^{119}Ba , in which two known bands based on opposite-parity orbitals [4]. The experimental data were obtained from a high-statistics experiment performed with γ -detector array JUROGAM 3 [6] coupled with the recoil mass separator MARA [7] employing the $^{58}\text{Ni}(^{64}\text{Zn}, 2pn)^{119}\text{Ba}$ reaction at 255 MeV beam energy. Several results on the structure of ^{119}Cs obtained from the same experiment have been recently published or submitted for publication [8–10]. Experimental details have been already included in those articles and therefore are not repeated here.

We report the following experimental results on ^{119}Ba : identification of a new positive-parity band and of several low-lying states, measurement of the half-life of the $5/2^-$ band-head of the $\nu h_{11/2}$ band, change of the high-spin part of the known positive-signature partner of the band built on the $\nu g_{7/2}[413]5/2^+$ orbital. We discuss the configurations of the observed bands, which are assigned based on the quasi-particle alignment analysis and on particle number conserving cranked shell model (PNC-CSM) calculations [11, 12].

* Present address: Key Laboratory of High Precision Nuclear Spectroscopy and Center for Nuclear Matter Science, Institute of Modern Physics, Chinese Academy of Sciences, Lanzhou 730000, People's Republic of China

† Deceased

II. EXPERIMENTAL RESULTS

The complete experimental information on the γ -ray transitions of ^{119}Ba is given in the Appendix. The level scheme including the previously known and the newly observed bands, as well as a zoom on the low-lying levels is shown in Figs. 1 and 2, respectively. Double-gated spectra obtained from prompt $\gamma\gamma\gamma$ coincidences showing the newly identified transitions are shown in Figs. 3 and 4. Spectra obtained from prompt-delayed coincidences of γ -rays detected by JUROGAM 3 and the detectors at the MARA focal plane are shown in Fig. 5.

The assignment of the bands to ^{119}Ba is based on the coincidence of the prompt $\gamma - \gamma$ coincidences with recoiling evaporation residues with mass 119 detected at the MARA focal plane, and with the 31 keV K_α and 35 keV K_β X-rays of barium nuclides detected in prompt coincidence with the in-band transitions by JUROGAM 3 array at the target position (see Fig. 2). The bands have been established based on coincidence relationships, intensity balance of the states, and when possible, on the angular correlations of the observed γ -rays. We adopt spin-parity $5/2^-$ for the band-head of the negative-parity band, and $7/2^+$ for the second lowest state of the positive-parity band, in agreement with the previous assignments based on delayed proton emission and on systematics [13].

Band 1, previously assigned to ^{119}Ba in Ref. [4], is confirmed up to $55/2^-$. The 1266-keV transition observed in Ref. [4] and placed on the side of Band 1, is now placed on top of the $55/2^-$ state and becomes the highest transition of Band 1 (see Fig. 1). It was known that the state fed by the 60-keV transition has an isomeric character, because no prompt transitions depopulating it were observed. This state was assigned as the band-head, and a spin-parity $I^\pi = 5/2^-$ was assigned based on the systematics of the observed bands in odd-even Ba nuclei [4]. We searched for delayed transitions detected at the MARA focal plane in coincidence with the prompt transitions of Band 1 measured at the target position, and succeeded to identify three delayed transitions with energies 53, 59 and 66 keV, which are not in mutual coincidence and therefore have been placed in parallel feeding directly the $3/2^+$ ground state. This placement fixes the energy of the $5/2^-$ state at 66 keV, and assumes the existence of two states at 59 and 53 keV which are fed from by two unobserved low-energy transitions of 7 and 13 keV, respectively, from the 66-keV $5/2^-$ state. We extracted a half-life of $T_{1/2} = 0.36(2) \mu\text{s}$ from the fit of the time spectrum of the 66-keV transition, which is the strongest among the three delayed transitions (see Fig. 6). We could not perform angular correlation analysis of the events measured at the MARA focal plane. Therefore, the electromagnetic character of these transitions could not be established experimentally, but only tentatively assigned. In order to qualitatively account for the half-life of the $5/2^-$ isomer, we assigned spins and parities $3/2^-$ and $3/2^+$ to the 53- and 59-keV states, respectively, which lead to $M1$ and $E1$ character for the

13- and 7-keV transitions. The Weisskopf estimates for the partial half-lives associated to the depopulation via the 66-, 13- and 7-keV γ rays are 0.97 ps, 813 ps and 413 ps, their conversion coefficients are 0.7, 1.2 and 3.8, and their relative intensities are 0.7, 0.2 and 0.1, respectively. Assuming a hindrance factor of 10^{-6} for the 66- and 59-keV $E1$ transitions, the estimated half-life of the $5/2^-$ isomer is $0.56 \mu\text{s}$, in good agreement with the measured half-life of $0.36(2) \mu\text{s}$.

Band 2 was previously assigned to ^{119}Ba in Ref. [4], in which the states at the bottom of the band were not understood, and the spin-parity of the ground state could not be firmly assigned. However, based on the systematics of the positive-parity bands in odd-even Ba nuclei, a spin-parity $5/2^+$ was proposed based for the state depopulated by the 53-keV transition, which is confirmed by the present work and adopted as band-head of Band 2. We also report evidence of a new band, that we label Band 3, which decays via the 93- and 240-keV transitions to the same $3/2^+$ lowest level to which Band 2 decays via the 53- and 177-keV transitions. The spin and parity $I^\pi = 3/2^+$ of this lowest level fed by both Bands 2 and 3 are fixed by the angular correlations of the four feeding transitions from Bands 2 and 3, which have spins and parities assigned based on systematics and on the existence of several interconnecting transitions. We assign it as the band-head of Band 3 and the ground state of ^{119}Ba , which is in agreement with the previous assignment [13]. As discussed in the following, the configurations assigned to Bands 2 and 3, $\nu g_{7/2}[413]5/2^+$ and $\nu d_{5/2}[411]3/2^+$, respectively, are also in agreement with the adopted $5/2^+$ and $3/2^+$ band-heads of the two bands.

Seven out-of-band transitions are observed from the states of Band 2 towards states of Band 3 and towards the new $7/2^+$ state placed in-between Bands 2 and 3. The negative-signature partner of Band 2 is confirmed up to spin $75/2$ (see Figs. 1 and 4). The previously reported 361- and 364-keV transitions between the signature partner cascades, as well as the highest 1578-keV transition in the negative-signature partner [4], are not observed in the present experiment. The positive-signature partner of Band 2 is confirmed up to spin $29/2$, on top of which two transitions of 739 and 807 keV are placed. The previously reported 796-, 897- and 997-keV transitions in Ref. [4] are not confirmed. The presence of the 796- and 897-keV transitions in the spectra of Ref. [4] are most probably due to contamination from ^{115}I , a well populated nucleus via the $\alpha 3p$ reaction channel in the used reaction, and having a band with transitions of 411, 517, 622, 729, 797, 850, and 894 keV, while the presence of the 997-keV transition is probably due to the contamination from ^{116}Xe , a well populated nucleus via the $\alpha 2p$ reaction channel in the used reaction, and having the 524- and 616-keV transitions in the ground-state band, and the 998-keV transition in a Band 3 decaying to the ground-state band [13]. The absence of these transitions in the high-spin part of the positive-signature partner of Band 2 has important consequences: as will be discussed

Band 2

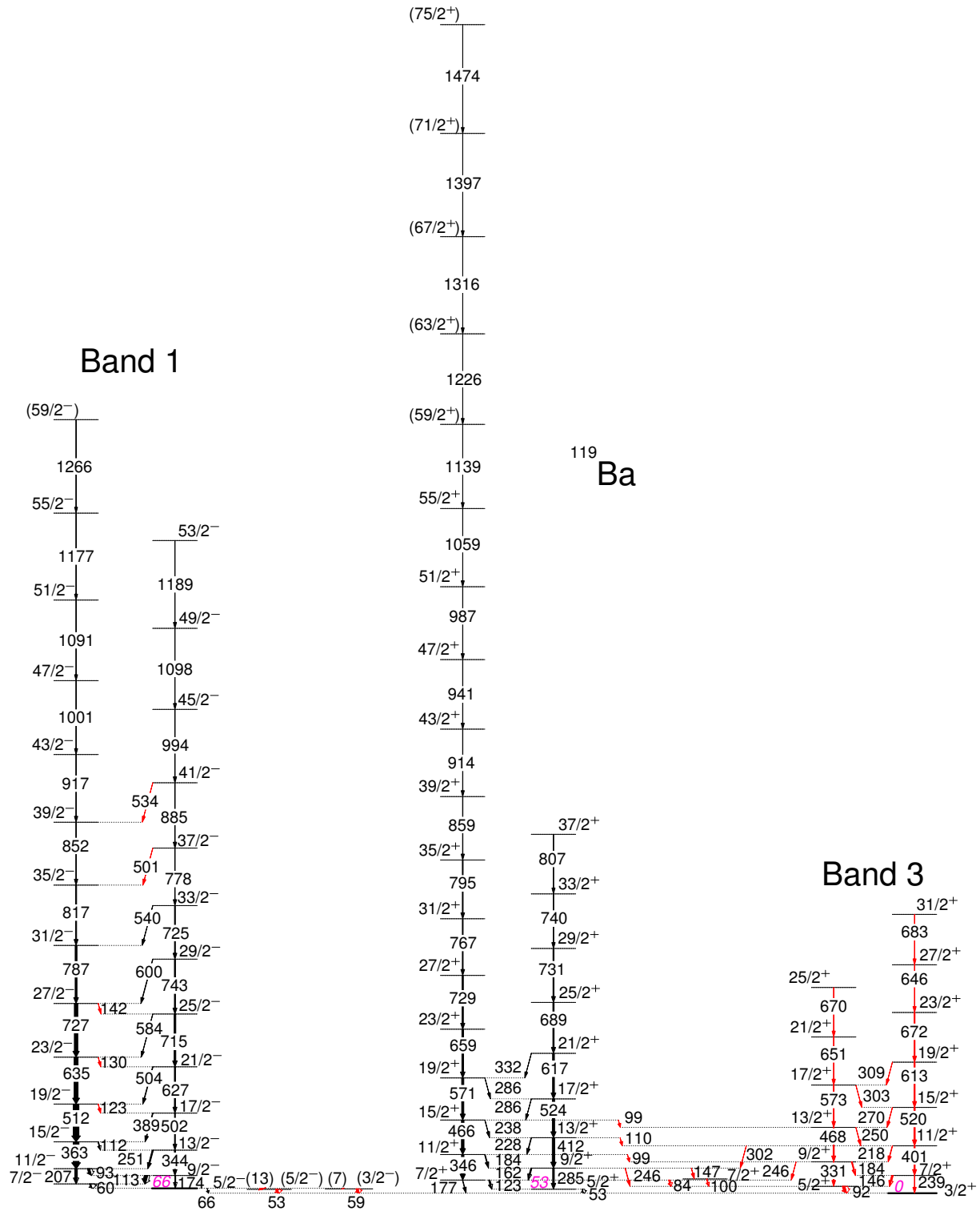


FIG. 1. (Color online) Level scheme of ^{119}Ba . The new transitions are indicated with red color. The isomeric levels are indicated with thick lines. The arrow widths are proportional the transition intensities.

[illegible]

Band 3 has been identified starting from the 84- and

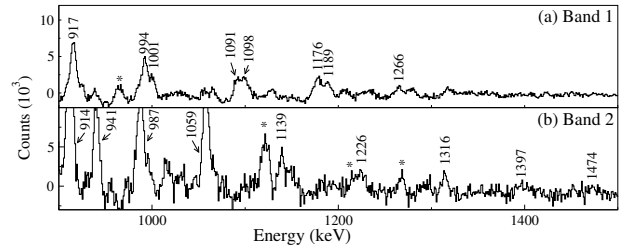


Figure 1 consists of four stacked gamma-ray spectra of ^{137}Ba , labeled (a) through (d). The x-axis for all plots is Energy (keV), ranging from 0 to 800. The y-axis is Counts, with different scales for each plot: (a) 10^3 , (b) 10^3 , (c) 10^2 , and (d) 10^2 .

- (a) Delayed transitions tagged with the 113-keV prompt transition of Band 1:** Shows peaks for Ba X-rays, 59, 66, and 66.
- (b) Band 1 transitions tagged with the 66-keV delayed transition:** Shows peaks for Ba X-rays, 60, 93, 112, 113, 174, 207, 251, 344, 363, 389, 502, 504, 512, 635, 715, 725, 727, 743, 787, and 66.
- (c) Band 1 transitions tagged with the 53-keV delayed transition:** Shows peaks for Ba X-rays, 60, 93, 112, 113, 174, 207, 251, 344, 363, 511, 635, 725, 727, 787, and 53.
- (d) Band 1 transitions tagged with the 59-keV delayed transition:** Shows peaks for Ba X-rays, 60, 93, 112, 113, 207, 363, 511, 635, 727, and 59.

92-keV transitions previously reported in Ref. [4] and placed in parallel to the other transitions depopulating the $7/2^+$ state of Band 2, but only after inverting their order. The 84-keV transition is now a connecting transition between Band 2 to the new Band 3, while the 92-keV transition becomes the lowest dipole transition in Band 3, which is built on the $3/2^+$ ground state. Band 3 is composed of two rotational cascades of $E2$ transitions connected by $M1/E2$ transitions. Their spins and positive parity are fixed by the 92-keV $M1/E2$ and 239-keV $E2$ transitions towards the $3/2^+$ band-head. Three out-of-band transition have been identified, two towards Band 2 and one towards the $7/2^+$ state depopulated by the 100-keV transition. The connecting transitions in both directions between Bands 2 and 3 indicate strong mixing between the states with identical spin, which differ in

energy by only a few tens of keV.

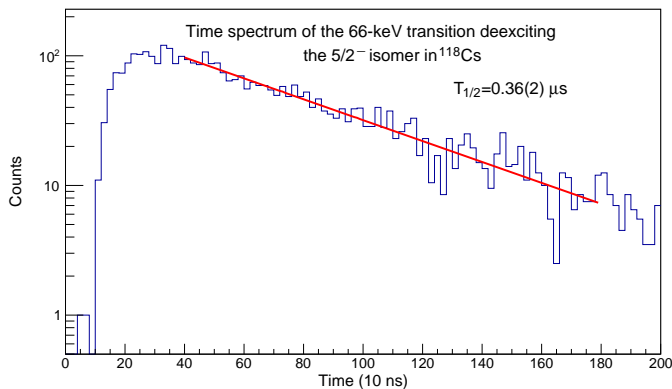


FIG. 6. (Color online) Fit of the time spectrum of the delayed 66-keV transition de-exciting the $5/2^-$ band-head of Band 1 of ^{119}Ba , measured at the MARA focal plane, and produced by gating on the 93-, 113-, 207-, and 363-keV transitions detected with JUROGAM 3 at the target position.

III. DISCUSSION

A. Alignment analysis

The quasi-particle alignments shown in Fig. 7 exhibit a large signature splitting between the signature partners of Band 1, and nearly degenerate signature partners in Bands 2 and 3.

The signature partners of the negative-parity Band 1 built on the $\nu h_{11/2}[541]3/2^-$ orbital exhibit alignments at a rotational frequency of $\hbar\omega \approx 0.35$ MeV. The alignment is due to $h_{11/2}$ protons, because the first $h_{11/2}$ neutron alignment predicted to occur at $\hbar\omega \approx 0.4$ MeV is blocked.

The alignment in the positive-parity Band 2 occurs at a similar rotational frequency of $\hbar\omega \approx 0.35$ MeV, and is higher by $\approx 1\hbar$ than that observed in Band 3, which is sharper, suggesting a lower deformation of Band 3 relative to that of Band 2. As Bands 2 and 3 are assigned to the $\nu d_{5/2}[413]5/2^+$ and $\nu g_{7/2}[411]3/2^+$ configurations (see the following section), respectively, one would expect a higher alignment in Band 3, which is in contrast with the experimental alignment which is smaller than in Band 2. However, as the two configurations assigned to the Bands 2 and 3 are strongly mixed, the K -values are difficult to define. An intermediate $K = 2$ value would lead to very similar alignments of the two bands. A second alignment is observed in Band 2 at $\hbar\omega \approx 0.46$ MeV, which was interpreted in Ref. [4] as due to $h_{11/2}$ neutrons. As the $\alpha = 1/2$ signature partner is populated up to a lower spin than the $\alpha = -1/2$ one, it is not clear if the alignment at $\hbar\omega \approx 0.46$ MeV is also present in the $\alpha = 1/2$ signature partner, even though the point at the highest frequency in Fig. 7 indicate the beginning of the expected second alignment.

In Figs. 8 and 9 we have drawn the alignments observed in the negative-parity and positive-parity bands in the sequence of light odd-even Ba nuclei from ^{117}Ba and ^{123}Ba . One can see the evolution of the alignments in the negative-parity bands which are sharper than in the positive-signature partners and increase with neutron number. Only in the negative-parity signature of Band 1 in ^{123}Ba a second alignment at $\hbar\omega \approx 0.6$ MeV has been observed. For the positive-parity bands we had to change the spins by two and one units in ^{121}Ba and ^{123}Ba , respectively, to get a gradual change of the alignment with increasing neutron number. One can observe similar alignment frequencies for all bands excepting Bands 3 of ^{119}Ba and ^{121}Ba , in which the alignments are also sharper. In ^{119}Ba the negative-signature partner of Band 3 was observed after the second alignment up to high spin. In ^{117}Ba , the alignment of negative-signature partner of Band 2 is more gradual, and no second alignment was observed.

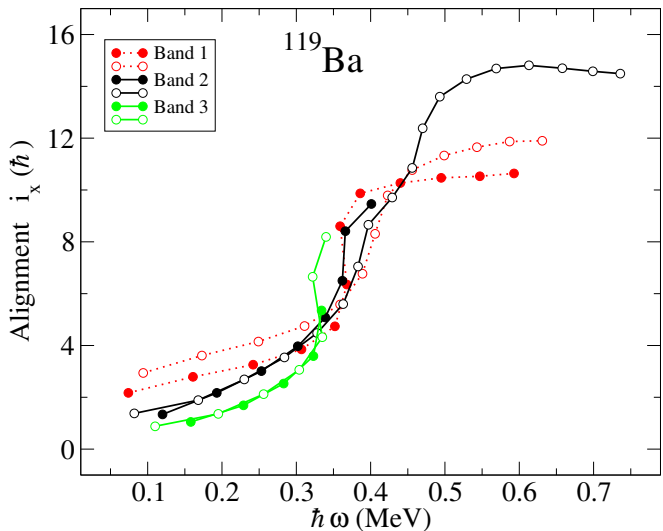


FIG. 7. (Color online) Single-particle alignments i_x for the bands of ^{119}Ba . The Harris parameters are $J_0 = 17 \hbar^2 \text{MeV}^{-1}$ and $J_0 = 25 \hbar^4 \text{MeV}^{-3}$. The K values are 2.5, 2.5, and 1.5 for Bands 1, 2, and 3, respectively. The states with signature $\alpha = +1/2$ and $\alpha = -1/2$ are drawn with filled and open symbols, respectively. The positive-parity and negative-parity bands are drawn with continuous and dotted lines, respectively.

B. PNC-CSM calculations

The possible configurations and alignment properties of the observed bands have been investigated through PNC-CSM calculations, in which the phenomenological Nilsson potential is adopted for the mean field [11], with parameters κ and μ taken from Ref. [14], and effective

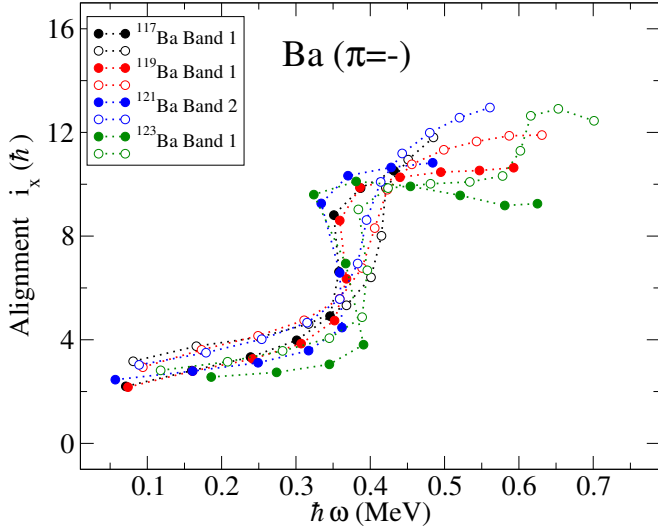


FIG. 8. (Color online) The same as in Fig. 7 but for the negative-parity bands of $^{117,119,121,123}\text{Ba}$. The K value is 2.5.

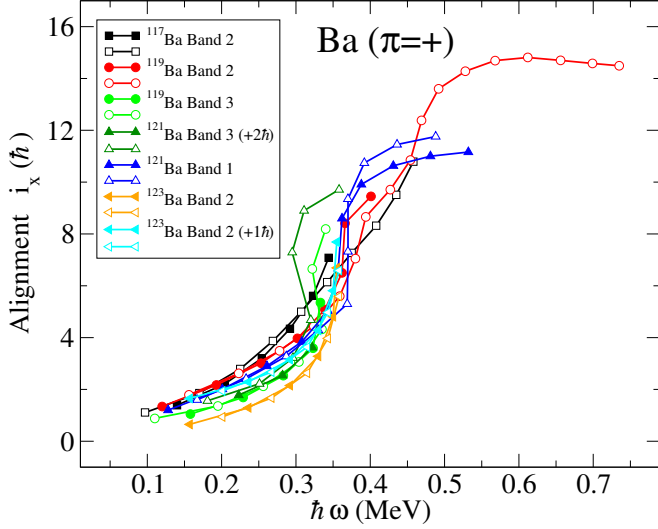


FIG. 9. (Color online) The same as in Fig. 7 but for the positive-parity bands of $^{117,119,121,123}\text{Ba}$. The K values are 1.5 for Bands 3 of $^{119,121}\text{Ba}$, and 2.5 for the other bands.

monopole pairing strengths of 0.8 MeV for protons and 0.6 MeV for neutrons. This model was recently used to successfully describe the band structure in rare-earth nuclei [12]. In the present analysis we compared the calculated moments of inertia $J^{(1)}$ and the projection of the angular momentum J_x on the cranking axis with the experimental values. Single-quasiparticle neutron Routhian diagrams as function of rotational frequency for prolate and

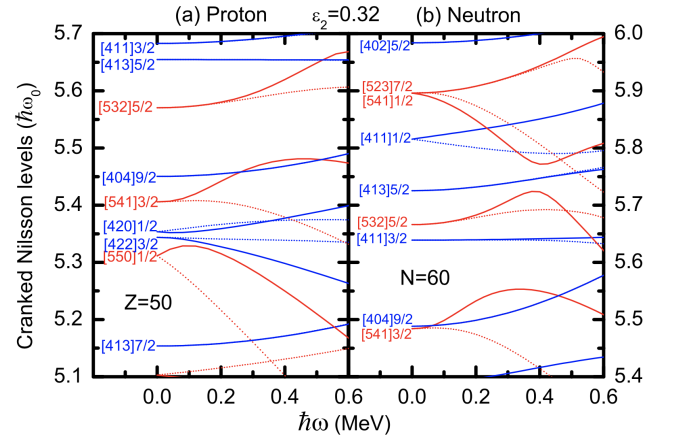


FIG. 10. (Color online) Single-particle Routhians located in the vicinity of the Fermi level of the ^{119}Ba as a function of rotational frequency for axial prolate deformation of $\varepsilon_2 = 0.32$: a) protons and b) neutrons. Positive (negative) parity Routhians are shown by blue (red) lines. Solid (dotted) lines are used for signature $\alpha = +1/2$ ($\alpha = -1/2$).

oblate deformations are shown in Fig. 10. They were used to guide the search of the closest quasiparticle orbitals to the proton and neutron Fermi surfaces.

The calculations were performed for an axial quadrupole deformation of $\varepsilon_2 = 0.32$, assumed to be equal to that resulting from the measured spectroscopic quadrupole moment of the neighboring ^{121}Ba nucleus [15, 16], but higher by about 20% than those resulting from total Routhian surface (TRS) calculations ($\varepsilon_2 = 0.27$) [3–5].

In order to find the deformation which best describes Band 1, we calculated the assigned $\nu[532]5/2^-$ configuration for different deformations of $\varepsilon_2 = 0.29, 0.32, 0.35$ (see Fig. 11). The calculated moments of inertia for a deformation of $\varepsilon_2 = 0.32$ leads to a good agreement for both signature partners. However, the alignments have a slightly different pattern in the two signature partners, being sharper and at lower rotational frequency in the $\alpha = 1/2$ partner. As one can see in Fig. 11, this can be induced by slightly different deformations, $\varepsilon_2 = 0.29$ for the $\alpha = 1/2$ partner and $\varepsilon_2 = 0.35$ for the $\alpha = -1/2$ partner, as expected, because a higher deformation induces higher crossing frequency. The larger deformation induced by the $\alpha = -1/2$ signature partner is also expected, since its Routhian has a larger slope and therefore a larger deformation driving force (see Fig. 10). The frequency of the observed up-bending at $\hbar\omega \approx 0.4$ MeV is well reproduced by the calculations, being induced by the alignment of $h_{11/2}$ protons. A second level crossing is predicted for the $\alpha = 1/2$ partner at $\hbar\omega \approx 0.7$ MeV, which is induced by $h_{11/2}$ neutrons, but is beyond the observed frequency range of Band 1 and therefore not confirmed. On the other hand, there is no second level crossing predicted for the $\alpha = -1/2$ partner.

Bands 2 and 3 are more difficult to reproduce by the

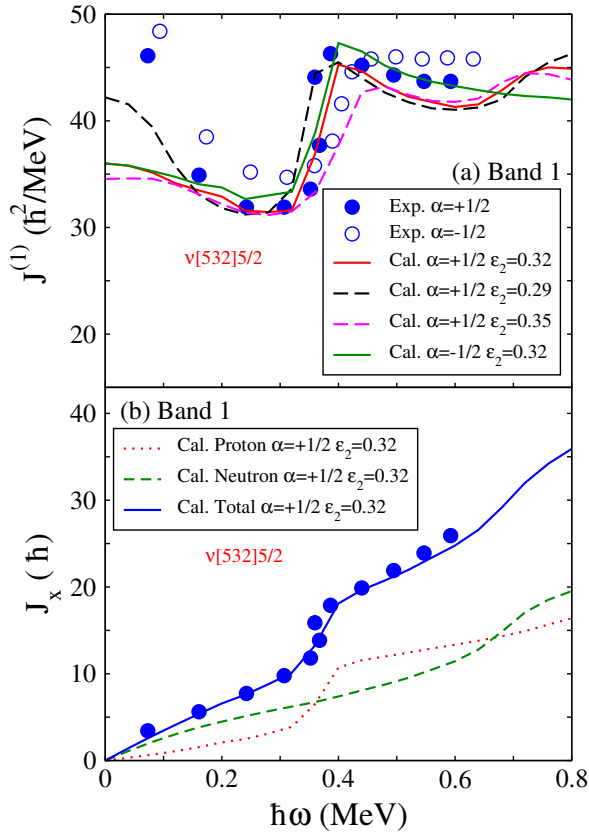


FIG. 11. (Color online) a) Moment of inertia $J^{(1)}$, b) projection of the angular momentum on the cranking axis J_x for Band 1 of ^{119}Ba calculated using the PNC-CSM model for deformation $\epsilon_2 = 0.32$. The states with signature $\alpha = +1/2$ and $\alpha = -1/2$ are drawn with filled and open symbols, respectively.

present PNC-CSM calculations, mainly due to the mixing between the two bands at low rotational frequency. It has been previously recognized that the configuration of the known positive-parity bands in Ba nuclei changes from $\nu g_{7/2}[402]5/2^+$ in ^{123}Ba to $\nu d_{5/2}[413]5/2^+$ in ^{121}Ba , in agreement with spectroscopic quadrupole moments measurements [15, 16]. The spectroscopic quadrupole moments of $^{117,119}\text{Ba}$ are not known experimentally. The $\nu d_{5/2}[413]5/2^+$ configuration assignment was based on TRS and cranked shell model calculations, which predict lower quadrupole deformations of $\epsilon_2 = 0.27$. However, even with the higher adopted deformation in the present calculations $\epsilon_2 = 0.32$, the $\nu d_{5/2}[413]5/2^+$ configuration assignment to the corresponding bands in $^{121,119}\text{Ba}$ remained unchanged, confirming the conclusion concerning the change of configuration from $\nu g_{7/2}[402]5/2^+$ in ^{123}Ba to $\nu d_{5/2}[413]5/2^+$ in the lighter $^{117,119,121}\text{Ba}$ nuclei. One can therefore discard the $\nu[402]5/2^+$ configuration for Bands 2 and 3, because it is far away from the Fermi surface (see Fig. 10). The $\nu[411]1/2^+$ orbital is closer to the Fermi surface, but it has very large signature split-

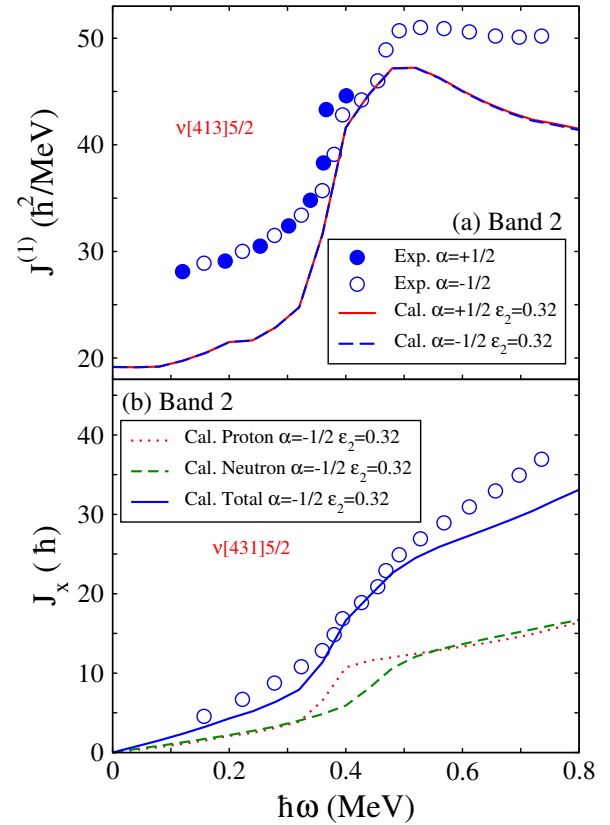


FIG. 12. (Color online) The same as in Fig. 11 but for Band 2 of ^{119}Ba .

ting, and therefore is inconsistent with the data. There remains only two positive-parity orbitals which are close to the Fermi surface and have small enough signature splitting in the low frequency region in agreement with the observed Bands 2 and 3: $\nu[411]3/2^+$ and $\nu[413]5/2^+$.

The two signature partners of Band 2 are quite similar up to the first up-bending observed at $\hbar\omega \approx 0.35$ MeV (see Fig. 7), which, based on the PNC-CSM calculations, is attributed to $h_{11/2}$ protons. The $\alpha = 1/2$ signature partner, which is observed up to much higher spin than the $\alpha = -1/2$ one, exhibits a second alignment at $\hbar\omega \approx 0.45$ MeV. As one can see in Fig. 12, the frequency of the first up-bending induced by $h_{11/2}$ protons is well reproduced, but the calculated $J^{(1)}$ is smaller than the experimental one. The frequency of the second alignment due to $h_{11/2}$ neutrons is also well reproduced. However, the behavior of the $\alpha = -1/2$ partner of Band 2 above the second alignment is not well reproduced: both the $J^{(1)}$ and J_x are smaller than the experimental values.

Band 3 is well reproduced by the $\nu[411]3/2^+$ configuration, except a bit higher calculated frequency of the up-bending induced by the alignment of $h_{11/2}$ protons (see Fig. 13).

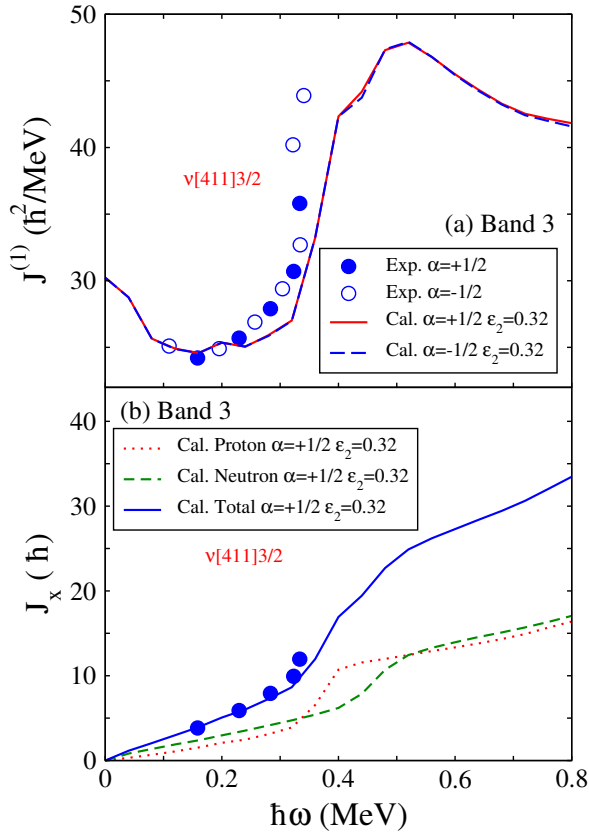


FIG. 13. (Color online) The same as in Fig. 11 but for Band 3 of ^{119}Ba .

IV. SUMMARY

The present work reports new results in ^{119}Ba , including one new band, several low-lying states and the half-

life measurement of the $5/2^-$ band-head of the $\nu h_{11/2}$ band. The puzzle of the different alignment patterns in the previously known positive-parity band is solved. The observed bands enrich the knowledge of the neutron single-particle excitations in very proton-rich lanthanide nuclei. Configurations are assigned based on the analysis of the alignment properties and on PNC-CSM calculations, which are in good agreement with experiment data and unveil the nature of the alignments observed in the different bands.

V. ACKNOWLEDGMENTS

This work has been supported by the China Scholarship Council (CSC), CSC No. 201804910386. This work has been supported by the Academy of Finland under the Finnish Centre of Excellence Programme (2012-2017), by the EU 7th Framework Programme Project No. 262010 (ENSAR), by the United Kingdom Science and Technology Facilities Council, by the National Research, Development and Innovation Fund of Hungary (Project No. K128947), as well as by the European Regional Development Fund (Contract No. GINOP-2.3.3-15-2016-00034); by the Polish National Science Centre (NCN) Grant No. 2013/10/M/ST2/00427; by the Swedish Research Council under Grant No. 2019-04880; and by the National Natural Science Foundation of China (Grants No. 11505242, No. 11305220, No. U1732139, No. 11775274, and No. 11575255). The use of germanium detectors from the GAMMAPOOL is acknowledged. I.K. was supported by National Research, Development and Innovation Office-NKFIH, contract number PD 124717.

-
- [1] I. Y. Lee, *Nucl. Phys. A* **520**, c641 (1990).
 - [2] N. Davids and D. Larson, *Nucl. Instr. Meth. Phys. Res. B* **40-41**, 1224 (1989).
 - [3] B. Ding *et al.*, *Phys. Rev. C* **95**, 024301 (2017).
 - [4] J. F. Smith *et al.*, *Phys. Rev. C* **61**, 044329 (2000).
 - [5] B. Cederwall *et al.*, *Nucl. Phys. A* **529**, 410 (1991).
 - [6] J. Pakarinen *et al.*, *Eur. Phys. J. A* **56**, 149 (2020).
 - [7] J. Sarén *et al.*, *Nucl. Instr. Meth. Phys. Res. A* **266**, 4196 (2008).
 - [8] K. K. Zheng *et al.*, chiral bands in ^{119}Cs , to be published.
 - [9] K. K. Zheng *et al.*, oblate-prolate coexistence in ^{119}Cs , to be published ().
 - [10] K. K. Zheng *et al.*, complete spectroscopy in ^{119}Cs , to be published ().
 - [11] J. Y. Zeng, T. H. Jin, and Z. J. Zhao, *Phys. Rev. C* **50**, 1388 (1994).
 - [12] Z. H. Zhang, M. Huang, and A. V. Afanasjev, *Phys. Rev. C* **101**, 054303 (2020).
 - [13] ENSDF, NNDC Online Data Service, ENSDF database, <http://www.nndc.bnl.gov/ensdf/>.
 - [14] T. Bengtsson and I. Ragnarsson, *Nucl. Phys. A* **436**, 14 (1985).
 - [15] S. A. Wells *et al.*, *Phys. Lett. B* **211**, 272 (1988).
 - [16] A. C. Mueller, F. Buchinger, W. Klempt, R. Otten, E. W. Neugart, and J. Ekström, C. Heinmeier, *Nucl. Phys. A* **403**, 234 (1983).
 - [17] K. Starosta *et al.*, *Nucl. Instrum. Meth. Phys. Res. A* **423**, 16 (1999).

VI. APPENDIX

TABLE I. Experimental information including the γ -ray energies E_γ , energies of the initial levels E_i , relative intensities I_γ , anisotropies R_{DCO} and/or R_{ac} , parameters a_2 and a_4 , polarization asymmetries A_p extracted following the prescription of Ref. [17], mixing ratios $\delta(M1/E2)$, multipolarities, and spin-parity assignments to the observed states in ^{119}Ba . The transitions listed with increasing energy are grouped in bands. The deduced values for R_{DCO} with a gate on stretched quadrupole transitions are ≈ 1 for stretched quadrupole and ≈ 0.46 for pure dipole transitions, while the ratio is close to 1 for a pure dipole and 2.1 for a stretched quadrupole transition when the gate is set on a pure dipole transition. The R_{ac} values for stretched dipole and quadrupole transitions are ≈ 0.8 and ≈ 1.4 , respectively.

E_γ (keV) ^a	E_i (keV)	I_γ^b	R_{DCO}^c	R_{ac}^d	a_2	a_4	A_p	δ	Mult.	$J_i^\pi \rightarrow J_f^\pi$
Band 1										
59.9	126.0	60(18)	1.0(1) ^f		-0.84(3)	0.46(5)		-1.8(4)	$M1/E2$	$7/2^- \rightarrow 5/2^-$
92.5	332.2	104(8)	0.40(7) ^e					-2.5(4)	$M1/E2$	$11/2^- \rightarrow 9/2^-$
112.1	695.4	18(5)	0.41(5) ^e					-2.6(5)	$M1/E2$	$15/2^- \rightarrow 13/2^-$
113.4	239.5	153(43)	0.53(6) ^e						$M1/E2$	$9/2^- \rightarrow 7/2^-$
122.6	1207.2	8(4)		0.9(2)					$M1/E2$	$19/2^- \rightarrow 17/2^-$
130.2	1842.0	3(1)							($M1/E2$)	$23/2^- \rightarrow 21/2^-$
142.3	2568.9	2(1)							($M1/E2$)	$27/2^- \rightarrow 25/2^-$
174.0	239.5	29(9)	1.9(9) ^f						$E2$	$9/2^- \rightarrow 5/2^-$
206.5	332.2	100	0.93(7) ^e				0.13(4)		$E2$	$11/2^- \rightarrow 7/2^-$
250.5	583.0	51(6)	0.9(1) ^f		-0.68(8)	0.18(14)	-0.02(1)	-0.20(30)	$M1/E2$	$13/2^- \rightarrow 11/2^-$
343.8	583.0	52(12)	2.2(3) ^f				0.06(2)		$E2$	$13/2^- \rightarrow 9/2^-$
363.2	695.4	254(48)	1.9(3) ^f				0.08(2)		$E2$	$15/2^- \rightarrow 11/2^-$
388.8	1084.5	28(9)		0.7(2)					$M1/E2$	$17/2^- \rightarrow 15/2^-$
500.5	4673.1	6(4)							($M1/E2$)	$37/2^- \rightarrow 35/2^-$
501.7	1084.5	38(11)	0.95(9) ^e						$E2$	$17/2^- \rightarrow 13/2^-$
504.1	1711.6	24(8)		0.7(2)					$M1/E2$	$21/2^- \rightarrow 19/2^-$
511.8	1207.2	254(50)	1.0(1) ^e				0.14(4)		$E2$	$19/2^- \rightarrow 15/2^-$
534.0	5558.1	2.7(9)							($M1/E2$)	$41/2^- \rightarrow 39/2^-$
539.8	3895.0	9(5)		0.9(1)					$M1/E2$	$33/2^- \rightarrow 31/2^-$
584.0	2426.5	9(3)		0.5(3)					$M1/E2$	$25/2^- \rightarrow 23/2^-$
600.4	3169.7	18(6)		0.6(2)					$M1/E2$	$29/2^- \rightarrow 27/2^-$
627.2	1711.6	51(28)	1.1(2) ^e						$E2$	$21/2^- \rightarrow 17/2^-$
634.8	1842.0	179(40)	1.2(2) ^e				0.11(3)		$E2$	$23/2^- \rightarrow 19/2^-$
715.0	2426.5	76(23)	1.3(2) ^e				0.08(4)		$E2$	$25/2^- \rightarrow 21/2^-$
725.3	3895.0	40(20)		1.3(3)					$E2$	$33/2^- \rightarrow 29/2^-$
726.9	2568.9	156(37)	1.0(2) ^e	1.3(1)			0.13(4)		$E2$	$27/2^- \rightarrow 23/2^-$
743.4	3169.7	50(31)	1.0(2) ^e						$E2$	$29/2^- \rightarrow 25/2^-$
778.1	4673.1	20(10)		1.5(3)					$E2$	$37/2^- \rightarrow 33/2^-$
786.5	3355.4	83(20)	1.0(1) ^f						$E2$	$31/2^- \rightarrow 27/2^-$
816.7	4172.1	48(13)	1.0(1) ^e						$E2$	$35/2^- \rightarrow 31/2^-$
851.6	5023.7	24(7)	1.0(2) ^e						$E2$	$39/2^- \rightarrow 35/2^-$
885.1	5558.1	22(12)		1.5(4)					$E2$	$41/2^- \rightarrow 37/2^-$
916.6	5940.3	19(11)		1.3(2)					$E2$	$43/2^- \rightarrow 39/2^-$
993.6	6551.7	19(10)		1.3(3)					$E2$	$45/2^- \rightarrow 41/2^-$
1000.7	6941.0	9(3)		1.4(3)					$E2$	$47/2^- \rightarrow 43/2^-$
1090.9	8031.9	6(3)		1.4(3)					$E2$	$51/2^- \rightarrow 47/2^-$
1097.6	7649.3	10(6)		1.3(4)					$E2$	$49/2^- \rightarrow 45/2^-$
1177.4	9209.3	6(2)		1.2(4)					$E2$	$55/2^- \rightarrow 51/2^-$
1188.9	8838.2	8(5)		1.6(5)					$E2$	$53/2^- \rightarrow 49/2^-$
1265.7	10475.0	4(2)							($E2$)	$(59/2^-) \rightarrow 55/2^-$
Band 1 \rightarrow Ground state										
(7.4)	66.0								($E1$)	$5/2^- \rightarrow (3/2^+)$
(12.6)	66.0								($E1$)	$5/2^- \rightarrow (3/2^-)$
53.4	53.4								($M1/E2$)	$(3/2^-) \rightarrow 3/2^+$
58.6	58.6								($E2$)	$(3/2^+) \rightarrow 3/2^+$
66.0	66.0								($E1$)	$5/2^- \rightarrow 3/2^+$
Band 2										
53.3	53.3	20(10)		0.7(1)					$M1/E2$	$5/2^+ \rightarrow 3/2^+$
123.1	176.5	45(9)	0.48(6) ^e					-1.6(1)	$M1/E2$	$7/2^+ \rightarrow 5/2^+$
161.5	338.2	53(12)	1.2(1) ^f				-0.14(5)	-2.3(2)	$M1/E2$	$9/2^+ \rightarrow 7/2^+$
177.0	176.5	17(3)		1.2(3)					$E2$	$7/2^+ \rightarrow 3/2^+$
183.9	522.3	28(9)	1.01(9) ^f				-0.02(1)	-2.5(5)	$M1/E2$	$11/2^+ \rightarrow 9/2^+$

TABLE I. (*Continued.*)

E_γ (keV) ^a	E_i (keV)	I_γ^b	R_{DCO}^c	R_{ac}^d	a_2	a_4	A_p	δ	Mult.	$J_i^\pi \rightarrow J_f^\pi$					
227.9	750.4	22(8)	0.53(9) ^e	0.8(1)			-0.11(5)		$M1/E2$	$13/2^+ \rightarrow 11/2^+$					
238.2	988.7	11(5)							$M1/E2$	$15/2^+ \rightarrow 13/2^+$					
285.0	338.2	71(30)	0.94(9) ^e						$E2$	$9/2^+ \rightarrow 5/2^+$					
285.5	1559.4	4(3)							($M1/E2$)	$19/2^+ \rightarrow 17/2^+$					
285.9	1274.7	5(4)							($M1/E2$)	$17/2^+ \rightarrow 15/2^+$					
332.2	1892.1	3(3)							($M1/E2$)	$21/2^+ \rightarrow 19/2^+$					
345.8	522.3	109(34)	0.86(7) ^e						$E2$	$11/2^+ \rightarrow 7/2^+$					
412.2	750.4	108(37)	0.94(9) ^e						$E2$	$13/2^+ \rightarrow 9/2^+$					
466.4	988.7	115(38)	1.01(6) ^e				0.06(2)		$E2$	$15/2^+ \rightarrow 11/2^+$					
524.3	1274.7	102(47)	1.18(9) ^e						$E2$	$17/2^+ \rightarrow 13/2^+$					
570.7	1559.4	96(40)	1.0(1) ^e						$E2$	$19/2^+ \rightarrow 15/2^+$					
617.4	1892.1	82(36)							$E2$	$21/2^+ \rightarrow 17/2^+$					
659.2	2218.6	76(38)	1.2(2) ^e	1.31(9)			0.11(6)		$E2$	$23/2^+ \rightarrow 19/2^+$					
688.7	2580.8	56(27)							$E2$	$25/2^+ \rightarrow 21/2^+$					
728.7	2947.3	57(30)	1.3(3) ^e						$E2$	$27/2^+ \rightarrow 23/2^+$					
731.4	3312.2	45(20)	1.1(3) ^e						$E2$	$29/2^+ \rightarrow 25/2^+$					
740.0	4052.2	15(8)		1.4(4)					$E2$	$33/2^+ \rightarrow 29/2^+$					
767.2	3714.5	35(19)		1.6(5)					$E2$	$31/2^+ \rightarrow 27/2^+$					
794.8	4509.3	35(20)		1.6(4)					$E2$	$35/2^+ \rightarrow 31/2^+$					
859.1	5368.4	16(9)		1.3(2)					$E2$	$39/2^+ \rightarrow 35/2^+$					
807.0	4859.2	8(4)		1.2(5)					$E2$	$37/2^+ \rightarrow 33/2^+$					
913.9	6282.3	11(7)		1.5(5)					$E2$	$43/2^+ \rightarrow 39/2^+$					
941.3	7223.6	10(7)		1.4(6)					$E2$	$47/2^+ \rightarrow 43/2^+$					
987.0	8210.6	9(5)		1.4(3)					$E2$	$51/2^+ \rightarrow 47/2^+$					
1059.3	9269.9	7(4)		1.3(4)					$E2$	$55/2^+ \rightarrow 51/2^+$					
1139.4	10409.3	4(2)							$E2$	$(59/2^+) \rightarrow 55/2^+$					
1225.6	11634.9	2(1)							$E2$	$(63/2^+) \rightarrow (59/2^+)$					
1315.8	12950.7	1.0(7)							$E2$	$(67/2^+) \rightarrow (63/2^+)$					
1397.0	14347.7	<1							$E2$	$(71/2^+) \rightarrow (67/2^+)$					
1473.9	15821.6	<1							$E2$	$(75/2^+) \rightarrow (71/2^+)$					
Band 2 \rightarrow Band 3															
84.4	176.5	32(6)	0.5(1) ^e									-2.3(4)	$M1/E2$	$7/2^+ \rightarrow 5/2^+$	
99.2	988.7	3(2)			($M1/E2$)	$15/2^+ \rightarrow 13/2^+$									
99.3	522.3	5(4)			($M1/E2$)	$11/2^+ \rightarrow 9/2^+$									
109.9	750.4	4(2)			($M1/E2$)	$13/2^+ \rightarrow 11/2^+$									
246.3	338.2	16(7)		1.4(4)					$E2$	$9/2^+ \rightarrow 5/2^+$					
Band 2 \rightarrow 7/2⁺															
146.5	338.2	12(5)		0.9(2)								-2.2(9)	$M1/E2$	$9/2^+ \rightarrow 7/2^+$	
7/2⁺ \rightarrow Band 3															
99.6	191.5	12(5)		0.5(2)									$M1/E2$	$7/2^+ \rightarrow 5/2^+$	
Band 3															
91.9	91.9	118(58)	0.5(1) ^e								-0.02(1)	-2(1)	$M1/E2$	$5/2^+ \rightarrow 3/2^+$	
146.3	238.4	56(20)	0.5(1) ^e										$M1/E2$	$7/2^+ \rightarrow 5/2^+$	
184.2	422.6	34(8)	1.3(3) ^f		0.8(2)			-0.16(9)					-3.8(6)	$M1/E2$	$9/2^+ \rightarrow 7/2^+$
217.5	639.9	18(7)												$M1/E2$	$11/2^+ \rightarrow 9/2^+$
238.9	238.4	17(9)	1.0(2) ^e	$E2$					$7/2^+ \rightarrow 3/2^+$						
249.8	890.2	9(4)		1.0(4)					$M1/E2$	$13/2^+ \rightarrow 11/2^+$					
269.6	1159.8	7(4)							($M1/E2$)	$15/2^+ \rightarrow 11/2^+$					
302.5	1462.7	4(2)							($M1$)/ $E2$	$17/2^+ \rightarrow 15/2^+$					
309.1	1772.3	<2							($M1/E2$)	$19/2^+ \rightarrow 17/2^+$					
330.8	422.6	31(6)	2.1(4) ^f						$E2$	$9/2^+ \rightarrow 5/2^+$					
401.4	639.9	50(13)	2.0(4) ^f				0.02(1)		$E2$	$11/2^+ \rightarrow 7/2^+$					
467.7	890.2	50(20)	1.7(3) ^f						$E2$	$13/2^+ \rightarrow 9/2^+$					
520.0	1159.8	57(26)	0.9(3) ^e						$E2$	$15/2^+ \rightarrow 11/2^+$					
572.6	1462.7	32(12)							1.2(3)	$E2$	$17/2^+ \rightarrow 13/2^+$				
612.5	1772.3	47(20)	1.2(2) ^e				0.02(2)		$E2$	$19/2^+ \rightarrow 15/2^+$					
645.8	3090.4	11(5)							1.3(3)	$E2$	$27/2^+ \rightarrow 23/2^+$				
650.8	2113.5	20(9)							1.4(3)	$E2$	$21/2^+ \rightarrow 17/2^+$				
670.2	2783.7	12(6)							1.6(5)	$E2$	$25/2^+ \rightarrow 21/2^+$				

TABLE I. (*Continued.*)

E_γ (keV) ^a	E_i (keV)	I_γ^b	R_{DCO}^c	R_{ac}^d	a_2	a_4	A_p	δ	Mult.	$J_i^\pi \rightarrow J_f^\pi$
672.3	2444.6	40(18)	1.0(2) ^e	1.4(2)					$E2$	$23/2^+ \rightarrow 19/2^+$
683.0	3773.4	7(3)		1.3(5)					$E2$	$31/2^+ \rightarrow 27/2^+$
Band 3 \rightarrow Band 2										
245.9	422.6	6(3)							($M1/E2$)	$9/2^+ \rightarrow 7/2^+$
302.2	639.9	5(2)							($M1/E2$)	$11/2^+ \rightarrow 9/2^+$

^aThe error on the transition energies is 0.3 keV for transitions below 500 keV, 0.7 keV for transitions between 500 and 1000 keV, and 1.0 keV for transitions above 1000 keV. The error on the transition transition energies is 1.0 keV for the transition intesities less 5.

^bRelative intensities corrected for efficiency, normalized to the intensity of the 206.5 keV, $11/2^- \rightarrow 7/2^-$ transition of Band 1. The transition intensities were obtained from a combination of total projection and gated spectra.

^c R_{DCO} has been deduced from an asymmetric $\gamma - \gamma$ coincidence matrix sorted with the detectors at 157.6° on one axis, and the detectors at $\approx 90^\circ$ on the other axis. The tentative spin-parity of the states are given in parentheses.

^d R_{ac} has been deduced from two asymmetric $\gamma - \gamma$ coincidence matrices sorted with the detectors at 133.6° and 157.6° on one axis, and the detectors at $\approx 90^\circ$ on the other axis. The tentative spin-parity of the states are given in parentheses.

^e DCO ratio from spectrum gated on stretched quadrupole transition.

^f DCO ratio from spectrum gated on stretched dipole transition.